Virology 409 (2011) 251–261

Contents lists available at ScienceDirect

Virology

journal homepage: www.elsevier.com/locate/yviro

Structural analysis provides insights into the modular organization of picornavirus IRES

Noemí Fernández [a], Ana García-Sacristán [b,c], Jorge Ramajo [a], Carlos Briones [b,c], Encarnación Martínez-Salas [a,*]

[a] Centro de Biología Molecular Severo Ochoa, Consejo Superior de Investigaciones Científicas, Universidad Autónoma de Madrid, Cantoblanco 28049 Madrid, Spain
[b] Laboratorio de Evolución Molecular, Centro de Astrobiología (CSIC-INTA), Carretera de Ajalvir Km. 4, 28850 Madrid, Spain
[c] Centro de Investigación Biomédica en Red de Enfermedades Hepáticas y Digestivas (CIBERehd), Spain

ARTICLE INFO

Article history:
Received 25 June 2010
Returned to author for revision
12 September 2010
Accepted 8 October 2010
Available online 5 November 2010

Keywords:
Translation initiation
Picornavirus
IRES
GNRA motif
SHAPE probing
RNA accessibility
DNA microarrays

ABSTRACT

Picornavirus RNA translation is driven by the internal ribosome entry site (IRES) element. The impact of RNA structure on the foot-and-mouth disease virus (FMDV) IRES activity has been analyzed using Selective 2'Hydroxyl Acylation analyzed by Primer Extension (SHAPE) and high throughput analysis of RNA conformation by antisense oligonucleotides printed on microarrays. SHAPE reactivity revealed the self-folding capacity of domain 3 and evidenced a change of RNA structure in a defective GNRA mutant. A modified RNA conformation of this mutant was also evidenced by RNA accessibility to oligonucleotides. Interestingly, comparison of nucleotide reactivity with RNA accessibility revealed that SHAPE reactive nucleotides corresponding to the GNRA motif were not accessible to their respective target oligonucleotides. The differential response was observed both in domain 3 and the entire IRES. Our results demonstrate distant effects of the GNRA motif in the domain 3 RNA conformation, and highlight the modular organization of a picornavirus IRES.

Introduction

Initiation of translation of picornavirus RNAs is driven by the internal ribosome entry site (IRES) element, a region within the 5′ untranslated region (5′UTR) that recruits the ribosomal subunits internally using a 5′ end-independent mechanism. IRES elements are present in a large variety of RNA viruses (Balvay et al., 2007; Filbin and Kieft, 2009; Lukavsky, 2009; Martinez-Salas et al., 2008). Nevertheless, and despite performing the same function, IRES elements differ in nucleotide sequence, RNA structure and trans-acting factors requirement. Even within the group of picornavirus RNAs, IRES elements are divergent in sequence and structure having been classified in four groups in terms of RNA structural organization (Belsham, 2009; Fernandez-Miragall et al., 2009). The large heterogeneity of RNA sequence and factor requirement poses many questions concerning our understanding of a general mechanism behind IRES function. Moreover, the diversity of the currently known IRES elements imposes serious problems to accurately predict the presence of IRES elements in eukaryotic mRNAs.

Despite the lack of conserved primary sequence, a typical attribute of picornavirus IRES structure is the presence of stable stem-loops, a property shared with other viral IRES elements (Martinez-Salas, 2008; Belsham, 2009; Lukavsky, 2009). In addition, a distinctive feature of picornavirus IRES is their long length, ranging from about 300 to 460 nt, presumably needed to generate a plethora of recognition motifs involved in the interaction with a large number of host factors regulating IRES-mediated translation initiation (Fitzgerald and Semler, 2009; Pacheco and Martinez-Salas, 2010). RNA structure plays a fundamental role in picornavirus IRES translation initiation. As it occurs in many other RNAs, compensatory substitutions in base-paired regions allowed secondary structure conservation during viral evolution in the field. Besides, functional analysis of nucleotide substitutions in conserved regions has proven extremely valuable for the identification of essential motifs required either at the primary sequence level, or as secondary structural elements (Martinez-Salas, 2008).

Foot-and-mouth disease virus (FMDV) is a picornavirus that causes a devastating disease worldwide (Grubman et al., 2008). Regulatory elements on the 5′ and 3′ untranslated regions of the FMDV genome control translation and replication of the viral RNA (Belsham and Brangwyn, 1990; Kuhn et al., 1990; Saiz et al., 2001; Lopez de Quinto et al., 2002; Serrano et al., 2006; Lawrence and Rieder, 2009). The IRES element of FMDV encompasses about 460 nts organized in five domains (Fig. 1A) with the peculiarity that domain 1 forms part of the *cis*-acting replication element (*cre*) (Mason et al., 2002). While the 5′ and 3′ end sequences of the IRES element determine the interaction with various translation initiation factors (eIFs) and other RNA-binding proteins (Kolupaeva et al., 1996; Lopez

* Corresponding author. Fax: +34 911964420.
E-mail address: emartinez@cbm.uam.es (E. Martínez-Salas).

0042-6822/$ – see front matter © 2010 Elsevier Inc. All rights reserved.
doi:10.1016/j.virol.2010.10.013

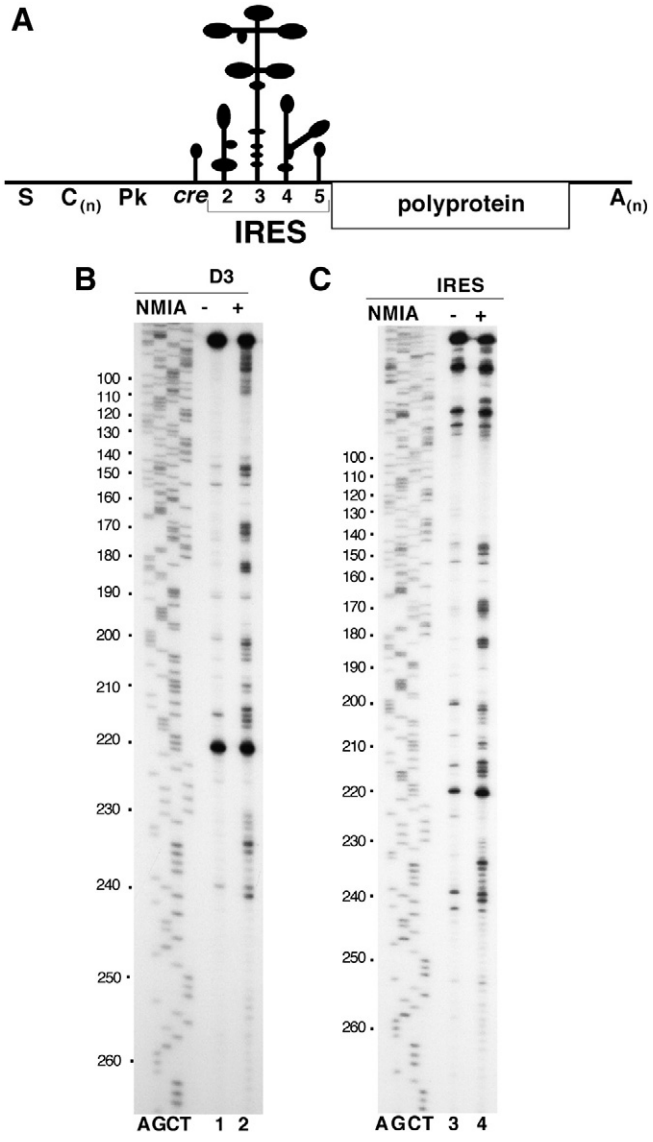

Fig. 1. SHAPE analysis of the FMDV IRES. (A) Schematic representation of the viral genome. Relevant features within the 5′ UTR are indicated; S stands for the S region, C (n) for poly C tract, Pk for pseudoknots, *cre* for cis-replicative element, and IRES for the internal ribosome entry site. IRES domains (2–5) referred to in the text are indicated; domain 1 overlaps with the *cre* element. The single open reading frame encodes a long polyprotein, flanked by a 3′UTR region with a poly(A) tail. (B) SHAPE analysis of the transcript domain 3 (D3). Primer extension analysis of RNA incubated with DMSO (−) or NMIA (+) conducted with a 5′-end labeled primer. Nucleotide positions are indicated on the left according to the sequencing lanes (AGCT) obtained with the same labeled primer; cDNA full-length products are shown at the top of each lane. (C) SHAPE analysis of the transcript encompassing the entire IRES, performed with the same labeled primer as in (B).

de Quinto and Martinez-Salas, 2000; Pilipenko et al., 2000; Lopez de Quinto et al., 2001; Stassinopoulos and Belsham, 2001; Andreev et al., 2007; Pacheco et al., 2008, 2009), the central region (termed domain 3, hereafter D3) contains RNA structural elements absolutely required for IRES activity (Lopez de Quinto and Martinez-Salas, 1997). In support of the essential role played by D3 during internal initiation, a transcript encompassing domains 4 and 5 does not possess IRES activity (Fernandez-Miragall et al., 2009), despite that it is endowed with the capacity to recruit translation initiation factors eIF4G, eIF4B, eIF3 and other IRES-binding factors.

The apical region of D3 in the IRES elements of encephalomyocarditis virus (EMCV) and FMDV contains two conserved purine-rich motifs, GNRA and RAAA (N stands for any nucleotide and R for purine). RNA structure studies have shown that the GNRA motif of FMDV, EMCV and poliovirus IRES adopts a tetraloop conformation at the tip of a stem-loop (Fernandez-Miragall and Martinez-Salas, 2003; Phelan et al., 2004; Du et al., 2004). Furthermore, as demonstrated by functional analysis, this motif is essential for IRES function (Lopez de Quinto and Martinez-Salas, 1997; Robertson et al., 1999).

The role played by D3 during IRES-dependent translation remains elusive. On the basis of its capacity to mediate intra-molecular and inter-molecular RNA-RNA interactions (Ramos and Martinez-Salas, 1999; Fernandez-Miragall et al., 2006), it has been proposed that this region instructs the functional conformation of the whole IRES element. In support of this idea, RNA probing analysis showed that mutations in the GNRA motif modified the RNA structure of this domain (Fernandez-Miragall and Martinez-Salas, 2003). Although RNA probing has provided important clues about the secondary structure of this region (Fernandez-Miragall et al., 2009) little is known about its three-dimensional structure.

RNA structure is tightly linked to biological function. Thus, as found in other RNA regulatory signals, the IRES secondary structure is phylogenetically conserved (Martinez-Salas, 2008). However, to understand the mechanism of IRES-dependent translation it is crucial to determine the spatial arrangement of the stem-loops shaping up its three-dimensional structural organization. We have previously used different chemical and enzymatic probes to gather information about the structure of FMDV IRES element in solution (Fernandez-Miragall et al., 2009). In order to deepen into the structure-function relationship of picornavirus IRES elements, we have undertaken the study of the FMDV IRES RNA structural organization using the wild type RNA sequence as well as a defective mutant carrying a single nucleotide substitution in the conserved GNRA motif. To this end, we have taken advantage of Selective 2′Hydroxyl Acylation analyzed by Primer Extension (SHAPE) reactivity. This method reveals flexible regions or nucleotides constrained in a conformation where the ribose 2′-OH is particularly susceptible to modification (Merino et al., 2005; Wilkinson et al., 2006; Vicens et al., 2007). In contrast, nucleotides involved in canonical base pairing or certain non-canonical but stable U:G, A:A, and A:G pairs have values of reactivity close to the background (Mortimer and Weeks, 2007). SHAPE analysis performed with the wild type IRES of FMDV verified our previous results regarding the RNA structure of D3 at the nucleotide level. Additionally, SHAPE reactivity studies demonstrated a change in RNA structure induced by the GUAG single nucleotide substitution at the GNRA motif that also affects the adjacent stem-loops within the apical region of D3. These results have been confirmed using an independent and complementary approach, with different level of resolution. High throughput analysis of RNA conformation by antisense oligonucleotide microarrays has been shown to be a sensitive method to detect structural differences in related RNA molecules (Duan et al., 2006; Kierzek et al., 2009; Mandir et al., 2009), including the 5′ end genomic regions of human immunodeficiency virus type 1 (HIV-1) (Ooms et al., 2004) and hepatitis C (HCV) (Martell et al., 2004). The study of the defective GUAG IRES mutant demonstrated discrete differences in RNA accessibility of distant stem-loops, also identified by SHAPE analysis. Together, the results obtained by SHAPE probing and RNA accessibility revealed a profound implication of the GNRA tetraloop in the FMDV IRES conformation and in its capacity to drive internal initiation.

Results

SHAPE analysis of IRES RNAs

To gain information about the RNA structure of the FMDV IRES we have performed a detailed RNA SHAPE analysis using wild type IRES transcripts and N-methylisatoic anhydride (NMIA) as the modifying agent (Wilkinson et al., 2006). SHAPE reactivity correlates inversely

with the probability that a nucleotide is base-paired or engaged in tertiary interactions, providing direct information of the RNA structure in solution (Merino et al., 2005). The result of primer extension analysis of the untreated (−) and NMIA-treated (+) D3 of the FMDV IRES is shown in Fig. 1B. Identification of the position of reverse transcriptase (RT) stops was achieved by the sequence loaded in parallel prepared with the same 5′ end-labeled primer. The untreated RNA was permissive to RT elongation with the exception of a non-specific intense RT-stop at nt 220 which was observed in all cases, and weak RT-stops at nts 145, 155, 190, 200 and 215. In turn, the treated RNA showed specific sharp RT-stops, specifically located between nts 140 to 253 of the IRES sequence (Fig. 1B).

Because of the high sensitivity at single nucleotide resolution of RNA SHAPE reactivity and the close relationship between structure and function of the IRES element, we wanted to assess how closely the structure of a transcript encompassing D3 alone resembled the same region in the context of the entire IRES. To this end, we analyzed the reactivity of D3 within the full-length IRES transcript. A similar pattern of reactivity was observed between nts 100 and 270 (Fig. 1C), indicating a very close RNA structure organization irrespective of the transcript used for SHAPE analysis. Taken together, these results demonstrate the presence of a similar pattern of RT-stops in both, D3 alone or the entire IRES, and confirm the existence of local flexible regions.

To quantify SHAPE reactivity in both transcripts, D3 and IRES, the intensity of each RT-stop measured by densitometry was normalized by the intensity of the full-length product in each lane. The signals in NMIA(−) lane were subtracted from the corresponding NMIA(+) lane. Then, the mean of three independent assays was calculated from the reactivity of each nt, made relative to the most reactive nt (set to 100%). The resulting D3 and IRES profiles, shown using step histograms (Fig. 2A, B) revealed that SHAPE reactivity was often associated in clusters of 3–6 nts. This is illustrated by the reactivity of nts 167–171, 181–183, 199–203, 209–216, or 230–240 in D3 transcript, strongly suggesting the presence of flexible regions within the IRES structure. Lack of SHAPE reactivity in nts 270–300 was observed using a primer annealing further downstream in the IRES transcript. Overall, the location of the most reactive nucleotides was in agreement with previous secondary structure data obtained using other modification agents (Fernandez-Miragall et al., 2009).

SHAPE analysis provided information about a large number of nts located all along the IRES element (Fig. 2C), for which experimental data were lacking and only predicted structures derived from RNA folding algorithms were available. Specifically, certain nts of domain 2, as well as domain 4, were highly reactive towards NMIA. This indicates the presence of flexible regions with hairpin loops and relatively large internal bulges, particularly clustered in motifs involved in the interactions with proteins that play an essential role during internal initiation (Martinez-Salas et al., 2008). Concerning domain 3, the reactivity obtained around nts 170, 200, 214, as well as 230–240, strongly supported the presence of bulges in this IRES region (Fig. 2C). Furthermore, SHAPE reactivity indicated that nts 180–182, unlike residues 177–179, were highly reactive towards NMIA. This result yielded new information about the reactivity of critical residues conforming the essential GNRA motif of the FMDV IRES. Additionally, nts 209–210 were reactive to NMIA, although these nts were previously predicted to be involved in C:G base pair formation (Fernandez-Miragall et al., 2009).

Most of the highly reactive residues in D3 were also hot spots in the entire IRES element (Fig. 2A, B). Despite the overall pattern of similar reactivity, differences observed at nts 95–107 were presumably induced by the presence of the upstream domains 1–2 in the IRES transcript, which may stabilize the structure of the basal region of D3. This result is in agreement with the mutational analysis performed within this IRES region (Martinez-Salas et al., 1996). Aside from highly reactive residues, the results of SHAPE analysis pointed towards the presence of two long non-reactive stretches encompassing nts 110–129 and 254–269 (Fig. 2C), compatible with a base-paired region within the central part of D3. Concerning the secondary structure of this particular IRES region, mutations leading to destabilization of the local base pairing within the stem of D3 impaired IRES activity (Serrano et al., 2009).

The data shown in Fig. 2A, B supported the interpretation that the RNA structure of D3 is an intrinsic feature of its own sequence. Therefore, we conclude that domain 3 is a self-folding region, barely affected by the presence of upstream or downstream domains of the IRES. This idea is in agreement with a division of functions among the domains of the IRES element (Serrano et al., 2009).

RNA accessibility detected by hybridization of IRES transcripts to antisense DNA oligonucleotides printed on microarrays

Because of the important implications of RNA structure organization in IRES activity (Martinez-Salas, 2008), we sought to assess whether IRES conformation could be detected by using a different approach. In recent times, hybridization of RNA molecules to antisense DNA oligonucleotide microarrays has been used as a method with the capacity to detect structural differences either in related viral RNA molecules or in different conformations of a given RNA molecule (Ooms et al., 2004; Martell et al., 2004). Thus, we first studied the accessibility of renatured RNAs encompassing domain 3 or the entire IRES to a panel of customized antisense oligonucleotides covering the entire sequence of the FMDV IRES element (see Material and methods and Supplemental Table 1).

RNA hybridization to microarrays of antisense DNA oligonucleotides was conducted using the fluorescent-labeled transcript corresponding to the full length IRES in native conditions (Fig. 3A). For this, *in vitro* transcribed RNA was labeled, renatured and hybridized to the printed oligonucleotides under the same ionic conditions and temperature used for SHAPE probing. In both transcripts, D3 and the full-length IRES, the normalized hybridization signal plotted against each oligonucleotide revealed RNA regions clearly accessible (mean accessibility value>0.4) (Fig. 3B) while others showed signals closer to the background (mean accessibility value<0.25). An intermediate accessibility window (0.25–0.4) presumably corresponded to regions with the potential to adopt RNA conformations with different accessibility in solution. The upper and lower thresholds were chosen on the basis of the mean values (± SD) of the most, or less, accessible regions, respectively.

Of interest, the pattern of accessibility of D3 either alone or within the entire IRES transcript showed a similar trend (Fig. 3B), confirming the conclusions derived from the SHAPE reactivity using these two transcripts. Only the oligonucleotide 288 in the 3′ border of the D3 RNA differed significantly in accessibility from that in the IRES transcript, presumably due to the influence of downstream IRES sequences, missing in transcript D3, in the folding of the spacer region that separates domains 3 and 4. Instead, the most accessible regions in both transcripts were complementary to oligonucleotides 99, 197, 239, 253 and 274, coincident with loops or bulges according to RNA SHAPE reactivity.

Relevant information can be extracted from the combination of the results obtained with two independent approaches, SHAPE RNA probing and accessibility to the oligonucleotides printed on microarrays. Overall, SHAPE reactive nts (Fig. 4A) matched accessible regions of D3 (corresponding to green or orange bars in Fig. 3B) revealed by microarrays. However, it is worth noting that three SHAPE reactive peaks (168–172, 182–184, and 213–216) reside within regions not accessible in the microarray analysis (Fig. 4B). This feature was also observed in the full-length IRES although in the later case, a fourth SHAPE peak (234–235) resided in a region of low accessibility to antisense oligonucleotides (Supplemental Fig. S1). Hence, one of the most notable differences between SHAPE

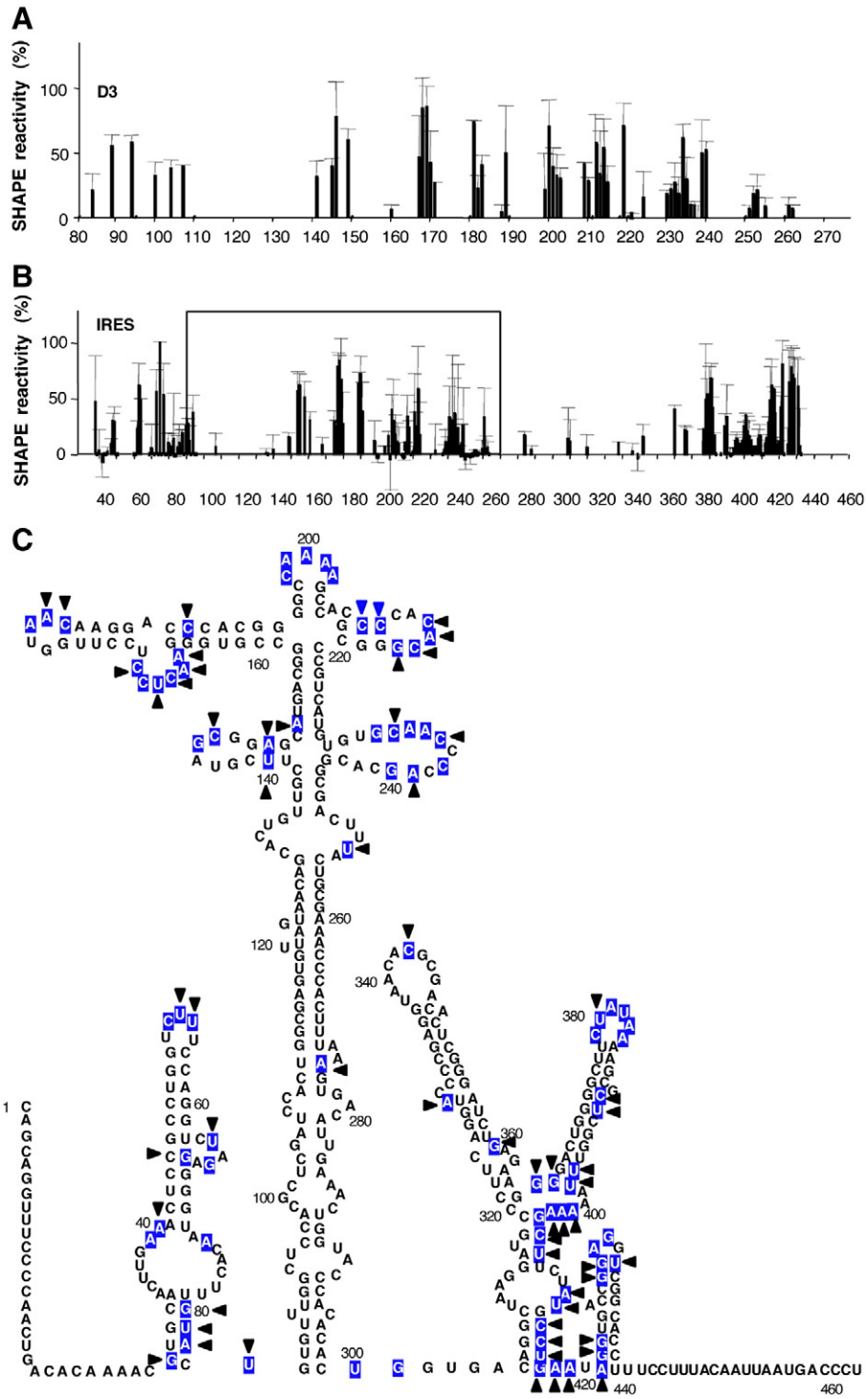

Fig. 2. SHAPE reactivity of IRES transcripts. (A) Histogram of domain 3 reactivity. Values correspond to the mean SHAPE reactivity (± SD) of three independent assays normalized to the intensity of the full-length cDNA product detected in the corresponding gel lane, followed by subtraction of the corresponding background RT-stop signal in the untreated RNA. (B) Histogram of full-length IRES transcript SHAPE reactivity. Nucleotide positions are indicated on the x-axis; nts corresponding to domain 3 are enclosed within a rectangle. (C) RNA structure of the FMDV IRES inferred from SHAPE reactivity. Nucleotides with SHAPE reactivity >0.10 are depicted by blue squares in the RNA secondary structure previously deduced from RNA probing. Black triangles point to nucleotides for which no RNA probing information was previously available.

reactivity and RNA accessibility mapped within the conserved GNRA motif previously proposed to participate in the RNA structure organization of D3 (Fernandez-Miragall and Martinez-Salas, 2003). As discussed below, this fact highlights the usefulness of the combined approach performed to analyze the RNA conformation of the IRES element.

Conserved motifs determine the local structure and activity of the IRES element

SHAPE analysis conducted with the wild type IRES transcript demonstrated that conserved motifs located in the apical region of domain 3, e.g., the GNRA motif around nts 178–182, the RAAA loop

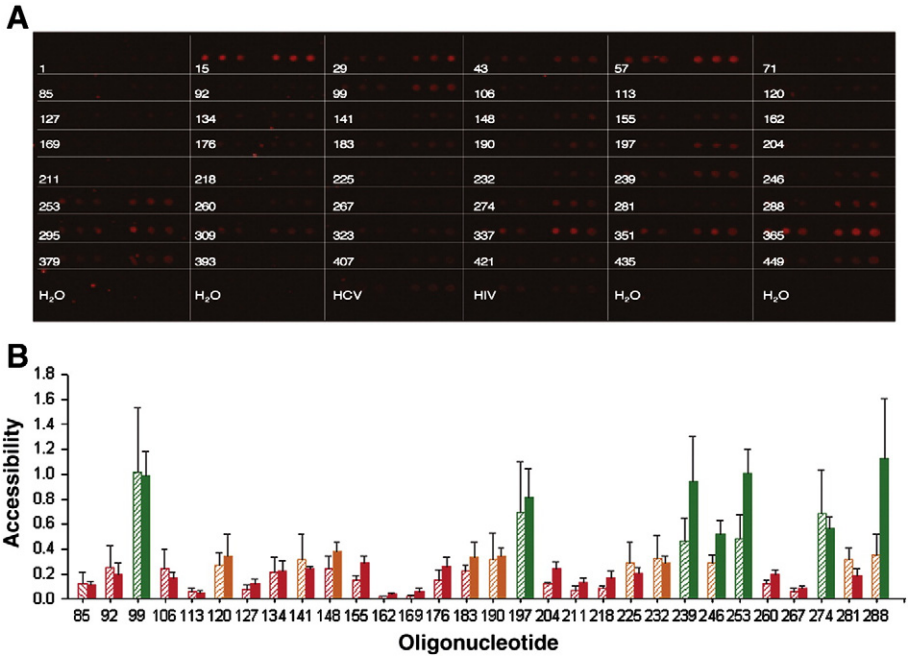

Fig. 3. Hybridization of IRES transcripts to antisense oligonucleotides printed on microarrays. (A) Hybridization signal of the fluorescence-labeled IRES transcript. The array contains 14-nt long antisense oligonucleotides (termed 1 to 449) complementary to the full IRES region, overlapping each 7 nt within the D3 (see Supplemental Table 1 for details). The bottom row contains negative controls (water and two oligonucleotides complementary to different regions of HCV and HIV-1 RNAs). (B) Comparison of the accessibility of D3 and IRES transcript. The fluorescent signal (mean ± SD), normalized to the intensity yielded by oligonucleotides 99 and 253, was plotted as a histogram for D3 (striped bars) and IRES (solid bars). Differences in accessibility are depicted in three colours: green (higher than 0.4), orange (range 0.4–0.25) and red (lower than 0.25). Differences in accessibility to oligonucleotides 239, 246, and 253 were not statistically significant ($P<0.1$, 0.025 and 0.025, respectively), whereas that of oligonocleotide 288 was significantly different ($P<0.005$).

around nts 199–203, 166–171 and 208–210 (Fig. 2C) were totally or partially reactive towards NMIA. The GNRA motif is fully conserved across 183 sequences of FMDV isolates (Table 1), and various mutations that disrupt the GNRA motif lead to severe decrease of IRES activity (Lopez de Quinto and Martinez-Salas, 1997). During the analysis of FMDV IRES sequence variability we noticed that certain nts located within flexible regions defined by SHAPE reactivity were phylogenetically invariant (Fig. 5A), suggesting a strong bias to maintain its primary sequence. To determine the contribution of some of these nts to IRES activity we analyzed the effect of substitutions in two invariant positions: A181 and G208. As expected because of its implication in the GNRA motif, the substitution A181G severely decreased IRES activity. In contrast, the mutation G208A did not alter IRES activity (Fig. 5B), suggesting that the primary sequence at this position is not required for activity. This result, together with the observed SHAPE reactivity of residues C209–C210 (Fig. 2C), indicated that residues located in the stem-loop spanning nts 208–117 adopt a flexible structure and confirmed the crucial contribution of the GNRA motif to IRES activity.

Conserved GNRA motifs often play a role in the tertiary folding on RNA molecules (Leontis et al., 2006; Geary et al., 2008). Thus, to reinforce the role of the GNRA motif in organizing the RNA structure of the IRES, we sought to assess the NMIA reactivity of the defective mutant GUAG that carries a single nt substitution A181G in the GNRA motif. Notably, SHAPE analysis of the RNA of this mutant showed enhanced NMIA reactivity of nts 180–182 (Supplemental Fig. S2) in comparison to the parental RNA, which carries the sequence GUAA in our FMDV C-S8 isolate (Fig. 5A), as it also occurs in most FMDV isolates (Table 1). Increase of SHAPE reactivity was in agreement with previous RNA probing data that indicated ribonuclease T1 accessibility to the mutated G181 in the GUAG IRES RNA (Fernandez-Miragall and Martinez-Salas, 2003).

RNA SHAPE analysis conducted in the context of the entire GUAG mutant IRES yielded similar results regarding the RNA structural organization of mutant D3 (Fig. 5C), with the exception of nts spanning the region 240–260 that were not reactive in the full-length IRES transcript because of the presence of background RT-stops in the untreated RNA (Supplemental Fig. S3A). SHAPE reactivity of the entire GUAG IRES indicated that RNA structure changes in comparison to the wt sequence tend to accumulate in similar positions within the transcript encompassing the individual domain 3 (Supplemental Fig. S3B), suggesting that the RNA reorganization affected mainly the central domain. This result highlighted the specific involvement of D3 in IRES activity, and the structural autonomy of this self-folding domain within the IRES.

Next, to confirm the modification of RNA structure of the GUAG IRES we analyzed the differential accessibility of the mutant IRES RNA to antisense oligonucleotides in the microarray assay. As shown in Fig. 6A, the accessibility of the mutant GUAG D3 and the corresponding IRES transcript displayed a similar trend. We then focused our attention to the region that was differentially affected in SHAPE reactivity in order to map the regions within the GUAG D3 that showed major changes in their accessibility to the complementary oligonucleotides. Analyses of the GUAG D3 differential accessibility in comparison to the wild type transcript revealed differences greater than 60% in two distant regions (Fig. 6B). Specifically, oligonucleotides 162 and 169 (which were the less accessible ones both in wild type and GUAG D3) showed the highest differential accessibility with the wild type RNA. The higher accessibility in the GNRA stem-loop of the mutant was not counterbalanced by the fact that the oligonucleotide 169 contained one mismatch with its complementary sequence in the GUAG RNA. Moreover, two additional oligonucleotides (204 and 211), complementary to a downstream region, were more accessible in the mutant IRES than in the wild type one. The location of these regions in the secondary structure (Fig. 6C) strongly suggests a distant effect of the GNRA motif in the conformation adopted by downstream stem-loops within D3. Also in support of this long-range effect, enhanced SHAPE reactivity of nts 181–183 was accompanied by increased reactivity of nts 213, 216, 238, 254 and 256, as well as lack of or decreased reactivity in 13 positions spread around nts 141 to 252 (Fig. 6C). This change in SHAPE reactivity of the mutant RNA compared to the wild type demonstrated a modified RNA conformation of the apical region of D3.

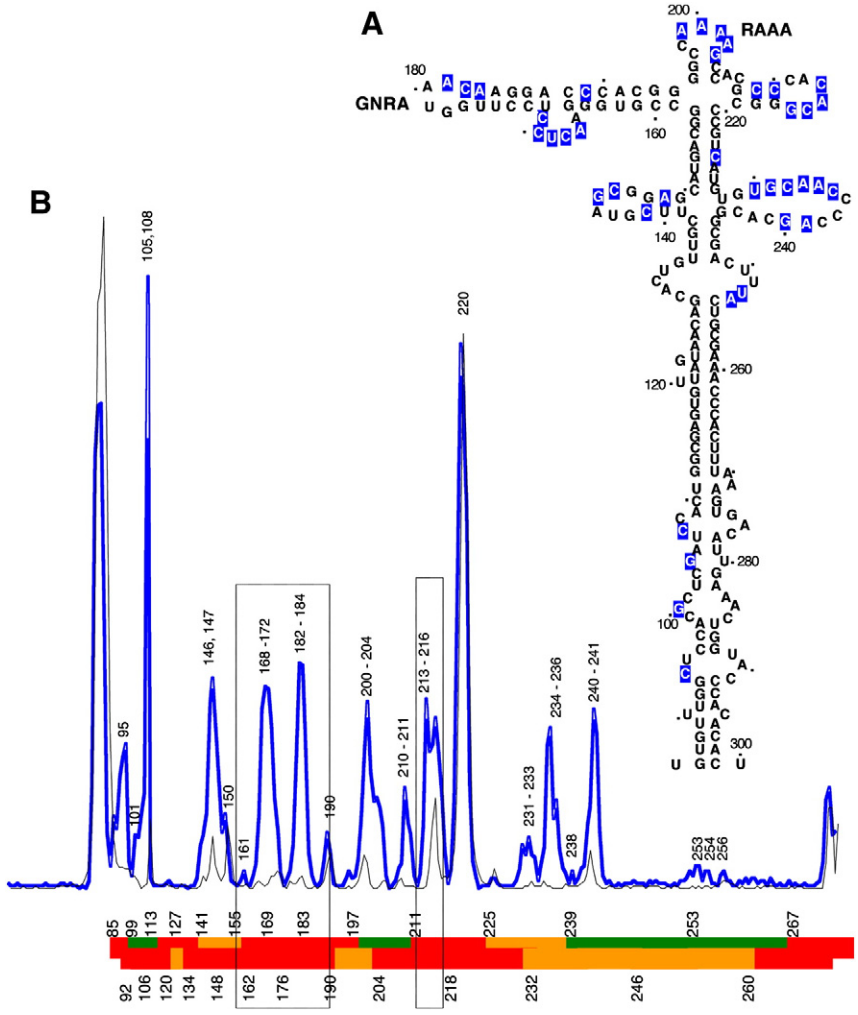

Fig. 4. Comparison of SHAPE reactivity with accessibility to oligonucleotides. (A) RNA structure of the FMDV IRES inferred from SHAPE reactivity. Nucleotides with SHAPE reactivity >0.10 are depicted by blue squares in the RNA structure, in conjunction with the secondary structure previously deduced from RNA probing. (B) Spectrum of a representative example of NMIA-treated (blue line) and DMSO-treated (black line) transcript D3. Numbers indicate the position of the RT-stop, that precedes by 1 nt the SHAPE reactivity shown in (A). The SHAPE spectrum is aligned with the accessibility of transcript D3 to the oligonucleotides on the microarray assay. Color code of RNA accessibility is used as in Fig. 3B. Regions exhibiting a differential response regarding SHAPE reactivity and accessibility to oligonucleotides are indicated by rectangles.

Altogether, the integration of SHAPE reactivity and RNA accessibility of wild type and mutant IRES elements analyzed here strongly support a direct effect of residues GUAA, constituting the GNRA motif of the vast majority of FMDV IRES sequences deposited in data bases (Table 1), in determining the RNA conformation of the active IRES affecting two relatively distant regions in the secondary structure of domain 3.

Discussion

Picornavirus IRES elements belong to the most efficient group of regulatory RNAs endowed with the capacity to drive internal initiation of translation of the viral RNA. However, they are also the most complex IRES elements described to date, owing to their long RNA sequence and multiple host factor requirements (Martinez-Salas et al., 2008; Fitzgerald and Semler, 2009). IRES function is tightly linked to its RNA structure (Martinez-Salas, 2008; Belsham, 2009; Lukavsky, 2009). Hence, solving the RNA structural organization of picornavirus IRES elements, in conjunction with the identification of the IRES-protein interacting network, is a challenge to understand how these specialized RNA structures perform their biological function.

In this study we took advantage of novel sensitive assays with the capacity to uncover differences in RNA conformation to assess changes in RNA structure of the IRES element in regions performing essential functions during internal initiation of translation. We have previously shown that the GNRA motif adopts a tetraloop conformation and mediates the local D3 RNA structure possibly involving tertiary interactions within this domain (Fernandez-Miragall and Martinez-Salas, 2003; Fernandez-Miragall et al., 2006), although the sequence acting as a potential GNRA receptor is not known yet. In RNAs whose three-dimensional structures are known, the GNRA tetraloop-receptor structures are organized in families of tertiary contacts, which depend on the nucleotide sequence of the tetraloop (Correll and Swinger, 2003; Geary et al., 2008; Depaul et al., 2010). In all cases, the interaction involves distant contacts between several bases of the tetraloop and specific residues in the receptor structure via non-canonical base pairing. The results of SHAPE reactivity (Fig. 2C) confirmed the existence of stem-loops whose structural

Table 1
Distribution of nucleotide sequences in the IRES GNRA motif of 183 isolates of FMDV belonging to the seven serotypes.

Sequence	A	C	O	ASIA	SAT 1,2,3	Number of isolates
GUAA	38	25	62	14	14	153
GUGA	1	0	5	10	4	20
GCGA	0	0	0	4	0	4
GCAA	0	0	1	4	0	5
GAGA	0	0	1	0	0	1

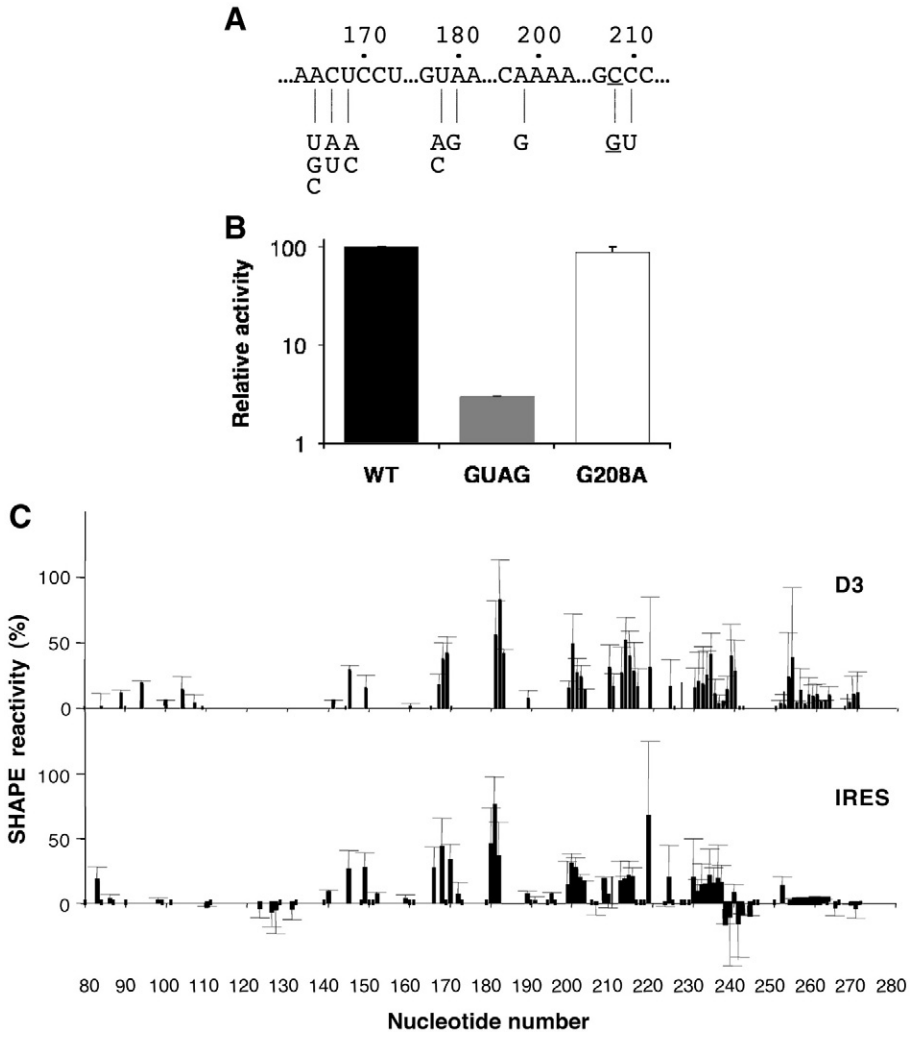

Fig. 5. Impact of the conserved GNRA motif in IRES activity and structure. (A) Nucleotide sequence variability found in 183 isolates of FMDV within flexible regions of the apical region of domain 3 defined by SHAPE reactivity. The reference sequence corresponds to FMDV C-S8 isolate. Underlined C209 indicates covariant substitution with nt 218. The invariant bases A181 and G208 were independently mutated to G and A respectively, and their relative IRES activity determined in BHK-21 transfected cells. (B). Relative IRES activity of mutants with nt substitutions A181G and G208A in the apical region of domain 3. (C) SHAPE reactivity of GUAG mutant IRES. Histograms of SHAPE reactivity obtained with D3 and IRES transcripts bearing a single nt substitution in the GUAA sequence to GUAG. Reactivity values correspond to the mean of three independent assays, normalized to the intensity of the full-length cDNA product. Nucleotide position is indicated on the *x*-axis.

conformation depends on specific residues of the GNRA motif (Fig. 6C). Thus, our results reinforced the idea that the nucleotides of the GNRA loop of the FMDV IRES could be involved in tertiary interactions with a region placed within D3.

The genetic variability of the FMDV IRES analyzed in 183 different isolates indicated that the tolerance in the sequence of this motif is always in accordance with the preservation of a GNRA motif [GUAA (83%), GUGA (10.9%), GCGA (2.2%), GCAA (2.7%), GAGA (0.5%)] (Table 1). These data also showed that there is a strong tendency to select for GUAA and GUGA in the FMDV IRES among all possible sequence combinations of its GNRA motif. As in many other RNAs, nucleotides engaged in base pair formation show covariation (Martinez-Salas, 2008; Gorodkin et al. 2010). However, the high degree of variability in other positions of the FMDV IRES, together with the fact that known GNRA tetraloop-receptor structures mainly correspond to GCAA, GAAA or GAGA sequences (Jaeger et al., 1994; Cate et al., 1996; Geary et al., 2008), imposes major difficulties to reveal nucleotide covariation indicative of tertiary interactions involving the GNRA motif, that is essential for initiation of translation in FMDV (Fig. 5B, Lopez de Quinto and Martinez-Salas, 1997). On the other hand, we can not rule out the possibility of having more than one GNRA tetraloop-mediated tertiary contact (Depaul et al., 2010), or that the disruption of tetraloop-receptor interaction may affect the formation of other tertiary contacts in the RNA (Chauhan and Woodson, 2008). Concerning the later possibility, a single substitution within the GNRA motif induced the reorganization of adjacent stem-loops (Fig. 6C). In support of the biological relevance of these changes for IRES activity, it is well established that conformational changes in RNA structure play a pivotal role in the function of many regulatory RNAs controlling gene expression. This is the case of the dicistrovirus intergenic region that determines internal initiation of the second cistron in the viral RNA (Pfingsten et al., 2010), the tRNA-shaped structure of plant RNA viruses that controls replication and translation of the viral genome (Zuo et al., 2010), the 5′ leader of HIV-1 that controls dimerization, polyadenylation and translation of the viral genome (Huthoff and Berkhout, 2001), and the RNA dimerization domain of the Moloney murine leukemia virus (Gherghe et al., 2010), among a long list of RNA regulatory elements.

Microarray analysis provided a different and complementary view of RNA structure by giving information about the accessibility of certain IRES regions to complementary DNA oligonucleotides. Although this method of analyzing IRES structure demonstrated an overall direct correlation with SHAPE reactivity, a key difference mapped within the conserved GNRA motif together with a

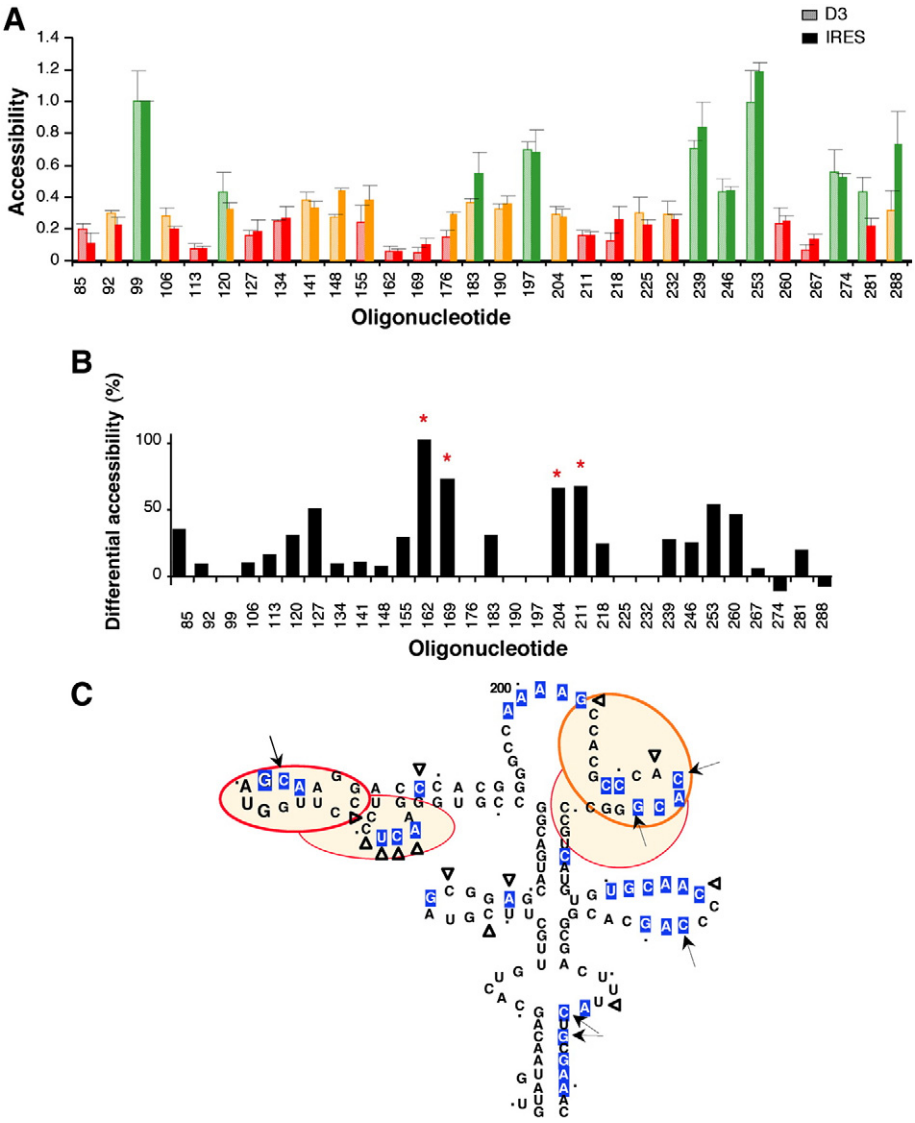

Fig. 6. Correlation between SHAPE reactivity and microarray-based accessibility in the mutant domain 3. (A) Accessibility of the GUAG IRES to antisense oligonucleotides printed on microarrays. The fluorescent signal (mean ± SD), normalized to the intensity yielded by oligonucleotides 99 and 253, was plotted as a histogram for D3 (striped bars) and the entire IRES (solid bars). Color bars are used as in Fig. 3B. (B) Differential accessibility of GUAG D3 transcript. The difference in the hybridization signal between the mutant sequence and the wild type, relative to the signal yielded by the parental RNA sequence, was plotted as a histogram. A red asterisk depicts differential accessibility larger than 60%. (C) RNA structure of the GUAG IRES deduced from SHAPE analysis. SHAPE-reactive nucleotides (> 0.10) are depicted by blue squares in the RNA structure, in conjunction with secondary structure deduced from RNA probing. Arrows depict nucleotides showing enhanced SHAPE reactivity (>50%) relative to the wild type RNA. Lack or decreased SHAPE (> 50%) reactivity compared to the wild type RNA is depicted by empty triangles. The regions showing the highest differential accessibility to oligonucleotides (> 60%, a subset of the oligonucleotides depicted by an asterisk in B) are highlighted by ovals.

downstream G:C base-paired region (Fig. 4A, B). Specifically, SHAPE reactive nts 181–183 and 209–216 were not accessible to their respective target oligonucleotides. This situation was also observed, though more moderate, in nts 230–240 (Supplemental Fig. S1B). The differences found can be explained by the biochemical properties of single nucleotide modification at its ribose 2′OH in solution versus the capacity of the region around these nts either to form base-pairs with the corresponding complementary region in the IRES or to competitively hybridize with the 14 nt-long oligonucleotides printed on the microarray. In particular, 3–4 consecutive nts within an RNA loop can show reactive ribose 2'OH groups, whereas their nucleobase positions prone to edge-to-edge base pairing can be compromised in the context of the entire molecule. Indeed, accessibility to DNA microarrays can inform simultaneously about the secondary and tertiary interactions within the target RNA molecule (Kierzek, 2009). Our study provides a proof of concept in favor of the use of accessibility to antisense oligonucleotide microarrays to measure RNA conformational changes, useful to understand the relationship between RNA structure and IRES activity. Although oligonucleotide microarrays lack the single nucleotide resolution provided by SHAPE or other chemical probing methods, they sense the local RNA conformation by its accessibility for base pairing, thus providing a high-throughput platform for straightforward structural analysis of IRES elements.

The comparison of SHAPE and RNA accessibility displayed by the mutant GUAG (Fig. 6C) further supported a change in RNA conformation affecting distant regions in the secondary structure of the FMDV IRES. It is worth noting that the enhanced SHAPE reactivity (> 50%) in the GUAG IRES mutant mapped within regions showing the highest differential accessibility to oligonucleotides (> 60%) (Fig. 6B). Taken together, our results show that domain 3 constitutes a self-folding RNA module inside the whole IRES element, and suggest that the nucleotides of the GNRA motif likely participate in tertiary intra-domain interactions, probably involving mechanisms other than complementary base pairing.

Materials and methods

In vitro transcription

The constructs expressing the IRES RNA (nts 1–462) of FMDV C-S8 or its D3 alone (nts 84–297) were previously described (Serrano et al., 2007). The defective IRES mutant carrying the substitution of A_{181} to G, disrupting the conserved GNRA motif, was described in (Lopez de Quinto and Martinez-Salas, 1997; Fernandez and Martinez-Salas, 2010). Plasmids were linearized to generate transcripts encoding D3, or the full-length IRES using restriction enzymes *Sma*I or *Xho*I, respectively. Transcription was performed for 2 h at 37 °C using 1000–3000 U of highly purified T7 RNA polymerase in the presence of 10–15 μg of linearized DNA template, 40 mM Tris–HCl, 50 mM DTT, 0.5 mM rNTPs. DNA template was eliminated by RQ1 DNase treatment (Promega), followed by phenol extraction and ethanol precipitation. Synthesis of full-length products and absence of contaminating DNA template was verified by gel electrophoresis. RNA concentration was determined by absorbance at 260 nm.

SHAPE analysis

RNA was treated with N-methylisatoic anhydride (NMIA) as previously described (Wilkinson et al., 2006) with some modifications. Prior to NMIA treatment, *in vitro* synthesized RNA (0.5 pmol in 3 μl of 0.5× TE), was renatured by heating at 95 °C for 2 min, snap-cooling on ice for 2 min, and incubation in a final volume of 4.5 μl of folding mix (100 mM HEPES pH 8.0, 6 mM $MgCl_2$, 100 mM NaCl) for 30 min at 37 °C. The RNA was split in two aliquots, adding 0.35 μl of NMIA (65 mM in DMSO) to one of them (NMIA+) and 0.35 μl of DMSO to the untreated control (NMIA-). Samples were incubated for 45 min at 37 °C. RNA was then precipitated and resuspended in 10 μl of 0.5× TE.

For primer extension, equal amounts of NMIA-treated and untreated RNAs (10 μl) were incubated with 0.5 μl of the appropriated antisense 5′ end ^{32}P-labeled primer (5′CTACGAAGCAACAGTG, 5′CCCGGGTGTGGGTACC, 5′GGAATGGGATCCTCGAGCTCAGGGTC) for 5 min at 65 °C, then 5 min at 35 °C and finally 1 min on ice. Extension was conducted in a final volume of 15 μl containing reverse transcriptase (RT) buffer (50 mM Tris–HCl pH 8.3, 3 mM $MgCl_2$, 75 mM KCl, 8 mM DTT), and 1 mM of each dNTP. The mix was heated at 52 °C for 1 min, prior to addition of 100 U of Superscript III RT (Invitrogen) and incubation at 52 °C for 30 min. Following template RNA hydrolysis with 0.75 μl of 4 M NaOH, cDNA products were recovered by ethanol precipitation. Dry pellets were resuspended in 10 μl of RNase-free H_2O with 4 μl of 90% formamide, 1 mM EDTA pH 8, 0.1% xilencianol, 0.1% bromophenol loading buffer. Heat-denatured cDNA products were fractionated in 6% acrylamide, 7 M urea gels, as described (Fernandez-Miragall and Martinez-Salas, 2007). A sequence obtained with the same primer was used to identify the RT stops after autoradiography of dry gels.

For SHAPE data processing, the intensities of RT-stops were quantified by densitometry, and normalized by the intensity of the full-length product in each lane. The signals in NMIA(−) lane were subtracted from the corresponding NMIA(+) lane, giving a 100% value to the most reactive nt. Subsequently, data from at least 3 independent assays were used to calculate the mean (± SD) SHAPE reactivity.

Microarray design and printing, RNA labeling, hybridization, and data analysis

Antisense DNA oligonucleotides complementary to the IRES element of FMDV were designed to hybridize against sequences of 14 consecutive bases of the IRES, overlapping each 7 bases in the case of D3 that was the focus of this study (Supplemental Table 1). Each oligonucleotide (named by the position on the IRES sequence complementary to the 3′ end of the primer) was composed of a C6 amino linker at its 5′ end, followed of a spacer consisting of five TCC repeats and the IRES antisense sequence at the 3′ end. Sequences and length of the oligonucleotides were designed to avoid formation of stable hairpins and to ensure proper hybridization with the IRES region. Two different primers with unrelated sequences (complementary to the 5′end of HCV and the RT region of the *pol* gene of HIV-1, and shown to lack sequence homology with FMDV IRES) were included in the study to provide a negative control in the hybridization signal. All oligonucleotides were diluted in 1× spotting solution (Telechem-Arrayit) and spotted onto epoxi-modified glass slides (Telechem-Arrayit). Microarrays containing 1,296 spots were printed in two duplicate grids per slide using a GMS 417 DNA arrayer (Affymetrix). Two concentrations (5 and 20 μM) of each oligonucleotide were printed in triplicate spots of 150 μm in diameter, with a distance of 300 μm between groups of triplicate spots.

The RNA was fluorescently labeled with Alexa 647 using the Ulysis 647 kit (Invitrogen). For this, RNA (1 μg) was incubated in 30 μl of labeling buffer for 15 min at 4 °C, prior to addition of 2 μl of the fluorescent dye. The labeling reaction was triggered by incubation of the mixture at 90 °C for 10 min. The sample was transferred to ice for 10 min, purified by Microcon (Millipore), and the final volume was adjusted to 10–15 μl in a speed vacuum. Absence of RNA cleavage was verified by denaturing gel electrophoresis.

Prior to hybridization, printed microarrays were washed in 2× SSC, 0.1% N-lauril sarcosine, for 2 min at room temperature, followed by 2 additional min in 2× SSC, as described (Martell et al., 2004; Martin et al., 2006). This step ensured the elimination of unbound DNA from the microarray surface, and the complete washing of the excess of spotting solution. Printed oligonucleotides were denatured by baking the slides for 2 min in boiling milli-Q water, then cooling for 10 sec at room temperature and immediately fixed in ice-cold 100% ethanol.

Microarrays were prehybridized in 6× SSC, 0.5% SDS and 10 μg/μl BSA for 45 min at 42 °C. Hybridization of the renatured fluorescent-labeled transcripts (300 ng) was performed in non-denaturing conditions with the same buffer used for SHAPE analysis (100 mM HEPES pH 7.5, 6 mM $MgCl_2$, 100 mM NaCl) for 2 h at 37 °C, using microarray hybridization chambers (Genetix). Slides were then washed twice, first in 1× washing buffer (20 mM HEPES pH 8.0, 6 mM $MgCl_2$, 50 mM NaCl) in the presence of 0.2% SDS for 15 min at room temperature, and then in washing buffer alone for 15 min at room temperature. After a final rinse with water, slides were dried by centrifugation for 1 min at 500g, and immediately scanned using a microarray scanner (Genepix 4100). Data were retrieved using the Genepix pro 6.0 software.

The differential capacity of transcripts for antisense oligonucleotide hybridization was measured in three independent experiments. In all cases, the raw fluorescence signal was corrected by subtraction of the local background. Microarrays data yielding a high background, displaying uneven fluorescent signal or showing hybridization signals in negative control points were discarded from further analysis. To compare the signal among the three independent hybridization assays conducted with different transcripts, the fluorescence signal yielded by the 20 μM spots were normalized to the intensity observed in the hybridization with oligonucleotides 99 and 253, which were the most intense in all cases. This allowed the correction for differences in RNA labeling and the normalization for differences in hybridization and washing steps.

The mean (± SD) of data derived from three microarrays was used to compare the differential capacity of transcripts to hybridize with each oligonucleotide in the array by calculating the ratio of the signal obtained in (mutant RNA - wt RNA) / wt RNA. Other normalizations such as the ratio (mutant RNA / wt RNA) yielded similar results, pointing to differences with the same oligonucleotides.

IRES activity

The GUAG mutant, carrying the substitution A181G, was described in (Lopez de Quinto and Martinez-Salas, 1997). In turn, the single substitution G208A was introduced using the pair of oligonucleotides 5′-GACGGGCCCGTGTGGGTGTGGCTTTTG-3′ (antisense) and 5′CGATGAGTGGCAGGGCGGGGC-3′ (sense). The PCR product was digested with *Eag*I and *Apa*I and inserted in the pBIC plasmid digested with the same enzymes. The nucleotide sequence of the entire amplicon was determined using automatic sequencing (ABI PRISM dye terminator cycle sequencing ready reaction kit, Perkin Elmer).

Relative IRES activity of FMDV IRES mutants A181G and G208A was quantified as the expression of luciferase normalized to that of chloramphenicol acetyltransferase (CAT) from bicistronic mRNAs (Martinez-Salas et al., 1993). Transfection of 80–90% confluent BHK-21 monolayers was carried out using cationic liposomes, 1 h after infection with the vaccinia virus recombinant vT7F-3 expressing the T7 RNA polymerase. Extracts from 1 to 2×10^5 cells were prepared 20 h postransfection in 100 µl of 50 mM Tris–HCl, pH 7.8, 120 mM NaCl, 0.5% NP40. Experiments were performed on triplicate wells and each experiment was repeated at least three times.

Supplementary materials related to this article can be found online at doi:10.1016/j.virol.2010.10.013.

Acknowledgments

We thank C. Gutierrez and D. Piñeiro for helpful comments. This work was supported by grants BFU-2008-02159, CSD-2009-00080 and by an Institutional grant from Fundación Ramón Areces. Work at Centro de Astrobiología was supported by MICINN (grants BIO2007-67523, EUI2008-00158), CSIC (grant 200920I040), European Union and Comunidad de Madrid. CIBERehd is funded by the Instituto de Salud Carlos III.

References

Andreev, D.E., Fernandez-Miragall, O., Ramajo, J., Dmitriev, S.E., Terenin, I.M., Martinez-Salas, E., Shatsky, I.N., 2007. Differential factor requirement to assemble translation initiation complexes at the alternative start codons of foot-and-mouth disease virus RNA. RNA 13, 1366–1374.

Balvay, L., Lopez Lastra, M., Sargueil, B., Darlix, J.L., Ohlmann, T., 2007. Translational control of retroviruses. Nat. Rev. Microbiol. 5, 128–140.

Belsham, G.J., 2009. Divergent picornavirus IRES elements. Virus Res. 139, 183–192.

Belsham, G.J., Brangwyn, J.K., 1990. A region of the 5' noncoding region of foot-and-mouth disease virus RNA directs efficient internal initiation of protein synthesis within cells: involvement with the role of L protease in translational control. J. Virol. 64, 5389–5395.

Cate, J.H., Gooding, A.R., Podell, E., Zhou, K., Golden, B.L., Kundrot, C.E., Cech, T.R., Doudna, J.A., 1996. Crystal structure of a group I ribozyme domain: principles of RNA packing. Science 273, 1678–1685.

Chauhan, S., Woodson, S.A., 2008. Tertiary interactions determine the accuracy of RNA folding. J. Am. Chem. Soc. 130, 1296–1303.

Correll, C.C., Swinger, K., 2003. Common and distinctive features of GNRA tetraloops based on a GUAA tetraloop structure at 1.4 A resolution. RNA 9, 355–363.

Depaul, A.J., Thompson, E.J., Patel, S.S., Haldeman, K., Sorin, E.J., 2010. Equilibrium conformational dynamics in an RNA tetraloop from massively parallel molecular dynamics. Nucleic Acids Res. 38, 4856–4867.

Du, Z., Ulyanov, N.B., Yu, J., Andino, R., James, T.L., 2004. NMR structures of loop B RNAs from the stem-loop IV domain of the enterovirus internal ribosome entry site: a single C to U substitution drastically changes the shape and flexibility of RNA. Biochemistry 43, 5757–5771.

Duan, S., Mathews, D.H., Turner, D.H., 2006. Interpreting oligonucleotide microarray data to determine RNA secondary structure: application to the 3' end of *Bombyx mori* R2 RNA. Biochemistry 45, 9819–9832.

Fernandez, N., Martinez-Salas, E., 2010. Tailoring the switch from IRES-dependent to 5'-end-dependent translation with the RNase P ribozyme. RNA 16, 852–862.

Fernandez-Miragall, O., Martinez-Salas, E., 2003. Structural organization of a viral IRES depends on the integrity of the GNRA motif. RNA 9, 1333–1344.

Fernandez-Miragall, O., Martinez-Salas, E., 2007. In vivo footprint of a picornavirus internal ribosome entry site reveals differences in accessibility to specific RNA structural elements. J. Gen. Virol. 88, 3053–3062.

Fernandez-Miragall, O., Ramos, R., Ramajo, J., Martinez-Salas, E., 2006. Evidence of reciprocal tertiary interactions between conserved motifs involved in organizing RNA structure essential for internal initiation of translation. RNA 12, 223–234.

Fernandez-Miragall, O., Lopez de Quinto, S., Martinez-Salas, E., 2009. Relevance of RNA structure for the activity of picornavirus IRES elements. Virus Res. 139, 172–182.

Filbin, M.E., Kieft, J.S., 2009. Toward a structural understanding of IRES RNA function. Curr. Opin. Struct. Biol. 19, 267–276.

Fitzgerald, K.D., Semler, B.L., 2009. Bridging IRES elements in mRNAs to the eukaryotic translation apparatus. Biochim. Biophys. Acta 1789, 518–528.

Geary, C., Baudrey, S., Jaeger, L., 2008. Comprehensive features of natural and in vitro selected GNRA tetraloop-binding receptors. Nucleic Acids Res. 36, 1138–1152.

Gherghe, C., Leonard, C.W., Gorelick, R.J., Weeks, K.M., 2010. Secondary structure of the mature ex virio Moloney murine leukemia virus genomic RNA dimerization domain. J. Virol. 84, 898–906.

Gorodkin, J., Hofacker, I.L., Torarinsson, E., Yao, Z., Havgaard, J.H., Ruzzo, W.L., 2010. De novo prediction of structured RNAs from genomic sequences. Trends Biotechnol. 28, 9–19.

Grubman, M.J., Moraes, M.P., Diaz-San Segundo, F., Pena, L., de los Santos, T., 2008. Evading the host immune response: how foot-and-mouth disease virus has become an effective pathogen. FEMS Immunol. Med. Microbiol. 53, 8–17.

Huthoff, H., Berkhout, B., 2001. Two alternating structures of the HIV-1 leader RNA. RNA 7, 143–157.

Jaeger, L., Michel, F., Westhof, E., 1994. Involvement of a GNRA tetraloop in long-range RNA tertiary interactions. J. Mol. Biol. 236, 1271–1276.

Kierzek, E., 2009. Binding of short oligonucleotides to RNA: studies of the binding of common RNA structural motifs to isoenergetic microarrays. Biochemistry 48, 11344–11356.

Kierzek, E., Christensen, S.M., Eickbush, T.H., Kierzek, R., Turner, D.H., Moss, W.N., 2009. Secondary structures for 5' regions of R2 retrotransposon RNAs reveal a novel conserved pseudoknot and regions that evolve under different constraints. J. Mol. Biol. 390, 428–442.

Kolupaeva, V.G., Hellen, C.U., Shatsky, I.N., 1996. Structural analysis of the interaction of the pyrimidine tract-binding protein with the internal ribosomal entry site of encephalomyocarditis virus and foot-and-mouth disease virus RNAs. RNA 2, 1199–1212.

Kuhn, R., Luz, N., Beck, E., 1990. Functional analysis of the internal translation initiation site of foot-and-mouth disease virus. J. Virol. 64, 4625–4631.

Lawrence, P., Rieder, E., 2009. Identification of RNA helicase A as a new host factor in the replication cycle of foot-and-mouth disease virus. J. Virol. 83, 11356–11366.

Leontis, N.B., Lescoute, A., Westhof, E., 2006. The building blocks and motifs of RNA architecture. Curr. Opin. Struct. Biol. 16, 279–287.

Lopez de Quinto, S., Martinez-Salas, E., 1997. Conserved structural motifs located in distal loops of aphthovirus internal ribosome entry site domain 3 are required for internal initiation of translation. J. Virol. 71, 4171–4175.

Lopez de Quinto, S., Martinez-Salas, E., 2000. Interaction of the eIF4G initiation factor with the aphthovirus IRES is essential for internal translation initiation in vivo. RNA 6, 1380–1392.

Lopez de Quinto, S., Lafuente, E., Martinez-Salas, E., 2001. IRES interaction with translation initiation factors: functional characterization of novel RNA contacts with eIF3, eIF4B, and eIF4GII. RNA 7, 1213–1226.

Lopez de Quinto, S., Saiz, M., de la Morena, D., Sobrino, F., Martinez-Salas, E., 2002. IRES-driven translation is stimulated separately by the FMDV 3'-NCR and poly(A) sequences. Nucleic Acids Res. 30, 4398–4405.

Lukavsky, P.J., 2009. Structure and function of HCV IRES domains. Virus Res. 139, 166–171.

Mandir, J.B., Lockett, M.R., Phillips, M.F., Allawi, H.T., Lyamichev, V.I., Smith, L.M., 2009. Rapid determination of RNA accessible sites by surface plasmon resonance detection of hybridization to DNA arrays. Anal. Chem. 81, 8949–8956.

Martell, M., Briones, C., de Vicente, A., Piron, M., Esteban, J.I., Esteban, R., Guardia, J., Gomez, J., 2004. Structural analysis of hepatitis C RNA genome using DNA microarrays. Nucleic Acids Res. 32, e90.

Martin, V., Perales, C., Abia, D., Ortiz, A.R., Domingo, E., Briones, C., 2006. Microarray-based identification of antigenic variants of foot-and-mouth disease virus: a bioinformatics quality assessment. BMC Genomics 7, 117.

Martinez-Salas, E., 2008. The impact of RNA structure on picornavirus IRES activity. Trends Microbiol. 16, 230–237.

Martinez-Salas, E., Saiz, J.C., Davila, M., Belsham, G.J., Domingo, E., 1993. A single nucleotide substitution in the internal ribosome entry site of foot-and-mouth disease virus leads to enhanced cap-independent translation in vivo. J. Virol. 67, 3748–3755.

Martinez-Salas, E., Regalado, M.P., Domingo, E., 1996. Identification of an essential region for internal initiation of translation in the aphthovirus internal ribosome entry site and implications for viral evolution. J. Virol. 70, 992–998.

Martinez-Salas, E., Pacheco, A., Serrano, P., Fernandez, N., 2008. New insights into internal ribosome entry site elements relevant for viral gene expression. J. Gen. Virol. 89, 611–626.

Mason, P.W., Bezborodova, S.V., Henry, T.M., 2002. Identification and characterization of a cis-acting replication element (cre) adjacent to the internal ribosome entry site of foot-and-mouth disease virus. J. Virol. 76, 9686–9694.

Merino, E.J., Wilkinson, K.A., Coughlan, J.L., Weeks, K.M., 2005. RNA structure analysis at single nucleotide resolution by selective 2'-hydroxyl acylation and primer extension (SHAPE). J. Am. Chem. Soc. 127, 4223–4231.

Mortimer, S.A., Weeks, K.M., 2007. A fast-acting reagent for accurate analysis of RNA secondary and tertiary structure by SHAPE chemistry. J. Am. Chem. Soc. 129, 4144–4145.

Ooms, M., Verhoef, K., Southern, E., Huthoff, H., Berkhout, B., 2004. Probing alternative foldings of the HIV-1 leader RNA by antisense oligonucleotide scanning arrays. Nucleic Acids Res. 32, 819–827.

Pacheco, A., Martinez-Salas, E., 2010. Insights into the biology of IRES elements through riboproteomic approaches. J. Biomed. Biotechnol. 2010, 458927.

Pacheco, A., Reigadas, S., Martinez-Salas, E., 2008. Riboproteomic analysis of polypeptides interacting with the internal ribosome-entry site element of foot-and-mouth disease viral RNA. Proteomics 8, 4782–4790.

Pacheco, A., Lopez de Quinto, S., Ramajo, J., Fernandez, N., Martinez-Salas, E., 2009. A novel role for Gemin5 in mRNA translation. Nucleic Acids Res. 37, 582–590.

Pfingsten, J.S., Castile, A.E., Kieft, J.S., 2010. Mechanistic role of structurally dynamic regions in Dicistroviridae IGR IRESs. J. Mol. Biol. 395, 205–217.

Phelan, M., Banks, R.J., Conn, G., Ramesh, V., 2004. NMR studies of the structure and Mg2+ binding properties of a conserved RNA motif of EMCV picornavirus IRES element. Nucleic Acids Res. 32, 4715–4724.

Pilipenko, E.V., Pestova, T.V., Kolupaeva, V.G., Khitrina, E.V., Poperechnaya, A.N., Agol, V. I., Hellen, C.U., 2000. A cell cycle-dependent protein serves as a template-specific translation initiation factor. Genes Dev. 14, 2028–2045.

Ramos, R., Martinez-Salas, E., 1999. Long-range RNA interactions between structural domains of the aphthovirus internal ribosome entry site (IRES). RNA 5, 1374–1383.

Robertson, M.E., Seamons, R.A., Belsham, G.J., 1999. A selection system for functional internal ribosome entry site (IRES) elements: analysis of the requirement for a conserved GNRA tetraloop in the encephalomyocarditis virus IRES. RNA 5, 1167–1179.

Saiz, M., Gomez, S., Martinez-Salas, E., Sobrino, F., 2001. Deletion or substitution of the aphthovirus 3' NCR abrogates infectivity and virus replication. J. Gen. Virol. 82, 93–101.

Serrano, P., Pulido, M.R., Saiz, M., Martinez-Salas, E., 2006. The 3' end of the foot-and-mouth disease virus genome establishes two distinct long-range RNA-RNA interactions with the 5' end region. J. Gen. Virol. 87, 3013–3022.

Serrano, P., Gomez, J., Martinez-Salas, E., 2007. Characterization of a cyanobacterial RNase P ribozyme recognition motif in the IRES of foot-and-mouth disease virus reveals a unique structural element. RNA 13, 849–859.

Serrano, P., Ramajo, J., Martinez-Salas, E., 2009. Rescue of internal initiation of translation by RNA complementation provides evidence for a distribution of functions between individual IRES domains. Virology 388, 221–229.

Stassinopoulos, I.A., Belsham, G.J., 2001. A novel protein-RNA binding assay: functional interactions of the foot-and-mouth disease virus internal ribosome entry site with cellular proteins. RNA 7, 114–122.

Vicens, Q., Gooding, A.R., Laederach, A., Cech, T.R., 2007. Local RNA structural changes induced by crystallization are revealed by SHAPE. RNA 13, 536–548.

Wilkinson, K.A., Merino, E.J., Weeks, K.M., 2006. Selective 2'-hydroxyl acylation analyzed by primer extension (SHAPE): quantitative RNA structure analysis at single nucleotide resolution. Nat. Protoc. 1, 1610–1616.

Zuo, X., Wang, J., Yu, P., Eyler, D., Xu, H., Starich, M.R., Tiede, D.M., Simon, A.E., Kasprzak, W., Schwieters, C.D., Shapiro, B.A., Wang, Y.X., 2010. Solution structure of the cap-independent translational enhancer and ribosome-binding element in the 3' UTR of turnip crinkle virus. Proc. Natl Acad. Sci. USA 107, 1385–1390.